Available online at www.sciencedirect.com
ScienceDirect
Journal of Computational Physics 222 (2007) 485–503
JOURNAL OF COMPUTATIONAL PHYSICS
www.elsevier.com/locate/jcp

A hybrid transport-diffusion method for Monte Carlo radiative-transfer simulations

Jeffery D. Densmore *, Todd J. Urbatsch, Thomas M. Evans, Michael W. Buksas

Transport Methods Group, Los Alamos National Laboratory, P.O. Box 1663, MS D409, Los Alamos, NM 87545, USA

Received 6 January 2006; received in revised form 25 July 2006; accepted 27 July 2006
Available online 11 September 2006

Abstract

Discrete Diffusion Monte Carlo (DDMC) is a technique for increasing the efficiency of Monte Carlo particle-transport simulations in diffusive media. If standard Monte Carlo is used in such media, particle histories will consist of many small steps, resulting in a computationally expensive calculation. In DDMC, particles take discrete steps between spatial cells according to a discretized diffusion equation. Each discrete step replaces many small Monte Carlo steps, thus increasing the efficiency of the simulation. In addition, given that DDMC is based on a diffusion equation, it should produce accurate solutions if used judiciously. In practice, DDMC is combined with standard Monte Carlo to form a hybrid transport-diffusion method that can accurately simulate problems with both diffusive and non-diffusive regions. In this paper, we extend previously developed DDMC techniques in several ways that improve the accuracy and utility of DDMC for nonlinear, time-dependent, radiative-transfer calculations. The use of DDMC in these types of problems is advantageous since, due to the underlying linearizations, optically thick regions appear to be diffusive. First, we employ a diffusion equation that is discretized in space but is continuous in time. Not only is this methodology theoretically more accurate than temporally discretized DDMC techniques, but it also has the benefit that a particle's time is always known. Thus, there is no ambiguity regarding what time to assign a particle that leaves an optically thick region (where DDMC is used) and begins transporting by standard Monte Carlo in an optically thin region. Also, we treat the interface between optically thick and optically thin regions with an improved method, based on the asymptotic diffusion-limit boundary condition, that can produce accurate results regardless of the angular distribution of the incident Monte Carlo particles. Finally, we develop a technique for estimating radiation momentum deposition during the DDMC simulation, a quantity that is required to calculate correct fluid motion in coupled radiation-hydrodynamics problems. With a set of numerical examples, we demonstrate that our improved DDMC method is accurate and can provide efficiency gains of several orders of magnitude over standard Monte Carlo.

Keywords: Radiative transfer; Monte Carlo; Hybrid transport-diffusion

* Corresponding author. Tel.: +1 505 665 9198.
E-mail addresses: jdd@lanl.gov (J.D. Densmore), tmonster@lanl.gov (T.J. Urbatsch), tme@lanl.gov (T.M. Evans), mwbuksas@lanl.gov (M.W. Buksas).

0021-9991/$ - see front matter
doi:10.1016/j.jcp.2006.07.031

1. Introduction

The Implicit Monte Carlo (IMC) method [1] has been shown to be an effective technique for solving non-linear, time-dependent, radiative-transfer problems via Monte Carlo simulation. In IMC, the absorption and emission of radiation by the material within a time step is approximated semi-implicitly by an effective scatter process. This effective scattering helps stabilize the calculation, allowing larger time steps than in a purely explicit method [2–4] (where radiation absorbed in a given time step cannot be re-emitted until the following time step). However, in optically thick regions, the mean-free path is small, and collisions are dominated by effective scatters. Thus, the transport process can be characterized as *diffusive*, and particles will suffer many collision during their lifetimes. These particle histories have an excessive number of steps and are expensive to process, a situation that results in a computationally inefficient Monte Carlo simulation.

Because of the diffusive nature of optically thick regions in IMC calculations, one would like to employ a hybrid method that uses standard Monte Carlo in optically thin regions of the problem and uses the diffusion approximation in optically thick regions. Ideally, this hybrid technique would produce accurate solutions while being more efficient than a pure Monte Carlo calculation. One such hybrid transport-diffusion method is based on the Random Walk (RW) technique [5,6]. In RW, several Monte Carlo steps are replaced by a macrostep over a spherical subregion of the cell centered about the particle's current position, thus increasing the efficiency of the simulation. Each RW step is governed by an analytic diffusion solution within the sphere, and the minimum allowable sphere radius (as measured in mean-free paths) is limited to ensure the accuracy of the diffusion solution. As a particle nears a cell boundary the radius of the sphere is reduced, RW is disabled, and the particle transports by standard Monte Carlo. When a spatial region is optically thin the radius of the sphere may never be sufficiently large enough to invoke RW, and particles will transport according to standard Monte Carlo only.

Discrete Diffusion Monte Carlo (DDMC) is another technique for increasing the efficiency of Monte Carlo simulations in diffusive media [7–10]. In DDMC, particles take discrete steps between spatial cells according to a discretized diffusion equation, with each discrete step replacing many small Monte Carlo steps. In practice, DDMC is combined with standard Monte Carlo to form a hybrid transport-diffusion method that can accurately simulate problems with both diffusive regions (where DDMC is used) and non-diffusive regions (where standard Monte Carlo is employed). Since a particle can travel to a new cell with each DDMC step (whereas RW is limited to a spatial subdomain within a cell), DDMC should be more efficient than RW.

Urbatsch et al. have developed a DDMC method for steady-state neutron transport problems [7], while the DDMC scheme of Evans, Urbatsch and Lichtenstein is designed to work with the equilibrium diffusion equation [8,11]. Gentile has successfully applied a method similar to DDMC (which he refers to as Implicit Monte Carlo Diffusion) to radiative-transfer calculations [9]. In this paper, we extend these previously developed DDMC techniques in three ways that improve the accuracy and utility of DDMC for planar-geometry, grey (i.e., frequency-independent) radiative-transfer simulations [10].

First, we employ a diffusion equation that is discretized in space but is continuous in time. In addition to being theoretically more accurate than temporally discretized DDMC implementations that use backward-Euler differencing [8,9], our methodology always retains the time of particle. Thus, there is no ambiguity regarding what time to assign a "DDMC particle" (i.e., a particle transporting in an optically thick region according to DDMC) that leaves an optically thick region and is converted into a "Monte Carlo particle" (i.e., a particle transporting in an optically thin region according to standard Monte Carlo). In contrast, other DDMC methods sample a time uniformly within the time step [9], and a particle may leave an optically thick region before it originally entered it, violating causality. This non-physical situation is avoided in our DDMC technique.

Second, we use an improved interface method for converting Monte Carlo particles incident on an optically thick region into DDMC particles [12,13]. This interface technique, which is based on the asymptotic diffusion-limit boundary condition [14], produces accurate solutions in the interior of optically thick regions regardless of the angular distribution of the incident radiation. Previous interface treatments that employ the Marshak boundary condition [7,8,15] can behave poorly if the incoming Monte Carlo particles are strongly anisotropic [12,13]. Also, Gentile uses an interface method that allows Monte Carlo particles to undergo several collisions in an optically thick region before converting these particles into DDMC particles

[9]. In addition to being inefficient because it uses Monte Carlo simulation in diffusive media, Gentile's technique can also produce erroneous results, especially if spatial cells are optically large [13].

Finally, we develop a scheme for determining radiation momentum deposition during the DDMC simulation. In coupled radiation-hydrodynamics problems, the correct calculation of fluid motion requires estimates of both the energy and momentum deposited in the material by the radiation [16,17]. The estimation of energy deposition is straightforward in both Monte Carlo and DDMC; when a particle is absorbed, its energy is allocated to the material. However, the calculation of momentum deposition in DDMC is difficult, since momentum is a direction-dependent quantity. DDMC is based on the diffusion approximation, therefore, DDMC particles have no angular information. To avoid this difficulty, we employ a momentum-deposition estimator that is based on the rate at which DDMC particles cross cell surfaces. Thus, angular information is extracted from the direction a particle travels to a new cell.

In the remainder of this paper we briefly overview the analytic equations governing planar-geometry, grey radiative transfer, the corresponding IMC method, and difficulties with IMC in optically thick regions. We then develop our improved DDMC technique and show how it can be combined with standard Monte Carlo in a hybrid transport-diffusion IMC simulation. Next, we use a set of numerical examples to demonstrate both the accuracy and improved efficiency, with respect to standard Monte Carlo and RW, of our new DDMC method. We conclude with a brief discussion.

2. Background

In the absence of internal sources and scattering, the planar-geometry, grey, radiative-transfer equations are [16–18]

$$\frac{1}{c}\frac{\partial I}{\partial t}+\mu\frac{\partial I}{\partial x}+\sigma I=\frac{1}{2}\sigma acT^4, \tag{1}$$

and

$$C_v\frac{\partial T}{\partial t}=\int_{-1}^{1}\sigma\left(I-\frac{1}{2}acT^4\right)\mathrm{d}\mu. \tag{2}$$

Here, $0<x<X$ is the spatial variable, $-1\leqslant\mu\leqslant 1$ is the angular variable, $t>0$ is the temporal variable, $I(x,\mu,t)$ is the radiation intensity, $T(x,t)$ is the material temperature, $\sigma(x,T)$ is the opacity, $C_v(x,T)$ is the heat capacity, a is the radiation constant, and c is the speed of light. To complete the problem description, appropriate initial conditions apply to I and T at $t=0$ and to I for incoming directions at the left ($x=0$) and right ($x=X$) boundaries.

In order to solve Eqs. (1) and (2) using IMC, we first prescribe a temporal grid $0=t_0<t_1<t_2<\cdots$ Then, within each time step $t_n<t<t_{n+1}$, the emission source on the right side of Eq. (1) is approximated semi-implicitly using Eq. (2). The resulting equations governing the IMC method are [1]

$$\frac{1}{c}\frac{\partial I}{\partial t}+\mu\frac{\partial I}{\partial x}+\sigma_n I=\frac{1}{2}(1-f_n)\sigma_n\int_{-1}^{1}I(x,\mu',t)\,\mathrm{d}\mu'+\frac{1}{2}f_n\sigma_n acT_n^4, \tag{3}$$

and

$$C_v\frac{\partial T}{\partial t}=\int_{-1}^{1}f_n\sigma_n\left(I-\frac{1}{2}acT_n^4\right)\mathrm{d}\mu, \tag{4}$$

where the subscript n refers to material properties evaluated at the beginning-of-time-step value of the temperature. In addition, the *Fleck factor* f_n is given by

$$f_n=\frac{1}{1+\beta_n c\sigma_n\Delta t_n}, \tag{5}$$

where

$$\beta_n=\frac{4aT_n^3}{C_{v,n}}, \tag{6}$$

and $\Delta t_n=t_{n+1}-t_n$ is the size of the time step.

For each time step, Eq. (3) can be solved for I using standard Monte Carlo simulation. The initial conditions are given by the prescribed initial radiation intensity and material temperature for the first time step, or by the results of the previous time step for subsequent time steps. Note that we have divided the explicitly evaluated physical opacity σ_n into an isotropic effective-scattering opacity $(1-f_n)\sigma_n$ and a corresponding effective-absorption opacity $f_n\sigma_n$. Thus, the IMC method approximates the absorption and emission of radiation within a time step by isotropic scattering. Accordingly, the emission source has been reduced by a factor of f_n. After I has been determined, the material temperature is updated using the radiation energy absorbed and emitted over the time step to evaluate Eq. (4).

In addition to the net radiation energy deposited in the material, coupled radiation-hydrodynamics calculations also require an estimate of the radiation momentum deposited in the material. The momentum deposition (i.e., the rate at which radiation momentum is deposited in the material per unit volume) corresponding to Eq. (1) is given in Refs. [16,17] by the equation

$$p(x,t) = \frac{\sigma}{c}\int_{-1}^{1} \mu I(x,\mu,t)\,\mathrm{d}\mu. \tag{7}$$

Integrals of this form can be estimated by Monte Carlo simulation in a straightforward manner. In this paper, we employ a track-length estimator [19] and approximate the opacity by its explicit value σ_n.

Eqs. (3) and (4) provide a systematic way of solving Eqs. (1) and (2) via Monte Carlo. However, in materials in which the opacity is large, the Monte Carlo simulation can become inefficient. Not only is the mean-free path between collisions small, but also, as we see from Eq. (5), the Fleck factor is small, and collisions are primarily effective-scattering events. Thus, the problem is highly diffusive, and Monte Carlo histories are extremely long. In the next section, we present a hybrid transport-diffusion technique for solving Eq. (3). In diffusive conditions, this hybrid method is much more efficient than standard Monte Carlo when the opacity is large but still yields accurate results.

3. Discrete diffusion Monte Carlo

We now develop the equations governing our improved DDMC method. This technique is based on the diffusion approximation to Eq. (3), so it should yield accurate solutions when used in appropriate regions (i.e., when σ_n is large and f_n is small). In addition, we will show that the DDMC transport process consists of discrete steps between spatial cells. Thus, DDMC should be more computationally efficient than a standard Monte Carlo simulation of Eq. (3).

We begin by considering a subregion $X_\mathrm{L} < x < X_\mathrm{R}$ of the problem domain that has been designated for simulation by DDMC. In this region, we develop a cell-centered discretization of the diffusion approximation corresponding to Eq. (3). This derivation is similar to the work of Szilard and Pomraning [20], except that we only discretize the spatial variable and treat time continuously. Integrating Eq. (3) over all directions yields

$$\frac{1}{c}\frac{\partial \phi}{\partial t} + \frac{\partial F}{\partial x} + f_n\sigma_n\phi = f_n\sigma_n acT_n^4, \tag{8}$$

where the scalar intensity is

$$\phi(x,t) = \int_{-1}^{1} I(x,\mu,t)\,\mathrm{d}\mu, \tag{9}$$

and the radiative flux is given by

$$F(x,t) = \int_{-1}^{1} \mu I(x,\mu,t)\,\mathrm{d}\mu. \tag{10}$$

Next, we divide the DDMC region into a spatial grid $X_\mathrm{L} = x_{1/2} < x_{3/2} < \cdots < x_{J+1/2} = X_\mathrm{R}$ consisting of J cells. If we integrate Eq. (8) over spatial cell j, we have

$$\frac{1}{c}\frac{\mathrm{d}}{\mathrm{d}t}\phi_j + \frac{1}{\Delta x_j}\left(F_{j+1/2} - F_{j-1/2}\right) + f_{n,j}\sigma_{n,j}\phi_j = f_{n,j}\sigma_{n,j}acT_{n,j}^4. \tag{11}$$

In Eq. (11), the cell-averaged scalar intensity is given by

$$\phi_j(t) = \frac{1}{\Delta x_j}\int_{x_{j-1/2}}^{x_{j+1/2}} \phi(x,t)\,\mathrm{d}x, \tag{12}$$

the cell-edge flux is

$$F_{j+1/2}(t) = F(x_{j+1/2}, t), \tag{13}$$

$\Delta x_j = x_{j+1/2} - x_{j-1/2}$ is the cell width, and we have used appropriate cell-averaged quantities for the material properties.

3.1. Interior cells

We continue our derivation of a cell-centered discretized diffusion equation for cells $2 \leqslant j \leqslant J-1$ in the interior of the DDMC region. We first evaluate the cell-edge fluxes using Fick's law [15,20]:

$$F_{j+1/2} = -\frac{1}{3\sigma_n}\frac{\partial\phi}{\partial x}\bigg|_{x=x_{j+1/2}}. \tag{14}$$

By employing a finite-difference approximation for Eq. (14), we can express $F_{j+1/2}$ in cell j as

$$F_{j+1/2} = -\frac{2}{3\sigma^-_{n,j+1/2}\Delta x_j}(\phi_{j+1/2} - \phi_j), \tag{15}$$

or in cell $j+1$ as

$$F_{j+1/2} = -\frac{2}{3\sigma^+_{n,j+1/2}\Delta x_{j+1}}(\phi_{j+1} - \phi_{j+1/2}). \tag{16}$$

In Eqs. (15) and (16), $\phi_{j+1/2}$ is an appropriately defined cell-edge scalar intensity. In addition, we have used a face-averaged value for the opacity in each cell. We will discuss the evaluation of these opacities later in this paper.

Next, equating Eqs. (15) and (16) and solving for the cell-edge scalar intensity yields

$$\phi_{j+1/2} = \frac{1}{\sigma^-_{n,j+1/2}\Delta x_j + \sigma^+_{n,j+1/2}\Delta x_{j+1}}(\sigma^+_{n,j+1/2}\Delta x_{j+1}\phi_j + \sigma^-_{n,j+1/2}\Delta x_j\phi_{j+1}). \tag{17}$$

Then, if we use Eq. (17) to evaluate either Eq. (15) or (16), we find that an approximate expression for the cell-edge flux is

$$F_{j+1/2} = -\frac{2}{3}\frac{1}{\sigma^-_{n,j+1/2}\Delta x_j + \sigma^+_{n,j+1/2}\Delta x_{j+1}}(\phi_{j+1} - \phi_j). \tag{18}$$

Substituting Eq. (18) and a similar expression for $F_{j-1/2}$ into Eq. (11) gives the DDMC equation for cells $2 \leqslant j \leqslant J-1$:

$$\frac{1}{c}\frac{\mathrm{d}}{\mathrm{d}t}\phi_j + (\sigma_{\mathrm{L},j} + \sigma_{\mathrm{R},j} + f_{n,j}\sigma_{n,j})\phi_j = f_{n,j}\sigma_{n,j}acT^4_{n,j} + \frac{1}{\Delta x_j}(\sigma_{\mathrm{L},j+1}\phi_{j+1}\Delta x_{j+1} + \sigma_{\mathrm{R},j-1}\phi_{j-1}\Delta x_{j-1}). \tag{19}$$

In Eq. (19), we have defined the left-leakage opacity as

$$\sigma_{\mathrm{L},j} = \frac{2}{3\Delta x_j}\frac{1}{\sigma^+_{n,j-1/2}\Delta x_j + \sigma^-_{n,j-1/2}\Delta x_{j-1}}, \tag{20}$$

and the right-leakage opacity as

$$\sigma_{\mathrm{R},j} = \frac{2}{3\Delta x_j}\frac{1}{\sigma^-_{n,j+1/2}\Delta x_j + \sigma^+_{n,j+1/2}\Delta x_{j+1}}. \tag{21}$$

We now give Eq. (19) a Monte Carlo interpretation. This equation can be viewed as a time-dependent infinite-medium transport problem for each cell. Thus, DDMC particles have no position or angular information, but always know their current cell and time. DDMC particles stream in time (but not in space) at the speed of light until experiencing a collision. To sample the time to collision τ, we first note that the time between collisions (as measured in mean-free times) is distributed exponentially, just as the distance between collisions (as measured in mean-free paths) in spatially dependent simulations. Thus, τ can be sampled in a way similar to the usual method of sampling distance to collision [19],

$$\tau = -\frac{1}{c}\frac{1}{\sigma_{\mathrm{L},j} + \sigma_{\mathrm{R},j} + f_{n,j}\sigma_{n,j}} \ln \xi. \tag{22}$$

Here, ξ is a random number uniformly distributed between 0 and 1, and the total opacity is given by the second term on the left side of Eq. (19) as $\sigma_{\mathrm{L},j} + \sigma_{\mathrm{R},j} + f_{n,j}\sigma_{n,j}$.

If the time to collision is less than the time remaining in the time step, the DDMC particle undergoes a collision, and the time to collision is decremented from the time remaining in the time step. Again, as we see from the second term on the left side of Eq. (19), a collision can be an absorption reaction, a left-leakage reaction, or a right-leakage reaction. The collision type is sampled from a histogram constructed from the relative magnitudes of the different opacities. If the collision is an absorption, the particle history is terminated, as in standard Monte Carlo. If the DDMC particle undergoes a leakage reaction, it is transferred to the appropriate neighboring cell, and the simulation continues.

If the time to collision is greater than the time remaining in the time step, the DDMC particle reaches the end of the time step and is stored for simulation in the next time step. Since, in the next time step, DDMC might not be used in the particle's cell, the DDMC particle is placed isotropically and spatially uniformly within the cell.

The right side of Eq. (19) contains the usual emission source term *and* source terms corresponding to DDMC particles experiencing leakage reactions in neighboring cells and being transferred to the current cell. These leakage source terms can be interpreted as the total rate at which radiation energy undergoes leakage reactions in adjacent cells (i.e., the leakage opacity multiplied by the cell-averaged scalar intensity multiplied by the cell volume) divided by the volume of the current cell such that the leaked radiation is distributed evenly over the cell.

It is interesting to note that as the opacity increases, not only do the leakage opacities decrease [from Eqs. (20) and (21)], but also, the absorption opacity $f_{n,j}\sigma_{n,j}$ is O(1) [from Eq. (5)]. Thus, from Eq. (22), the time between collisions is not excessively small, the collisions are primarily absorptions, and DDMC particle histories are relatively short. This situation is exactly the opposite effect that a large opacity has on a standard Monte Carlo simulation of Eq. (3).

We now discuss the evaluation of the face-averaged opacities in Eqs. (20) and (21). According to Szilard and Pomraning, if one of these opacities is very large, then the entire expression can be small, and radiation will not propagate [20]. This lack of propagation is commonly seen when the opacity is strongly temperature-dependent, and the material is cold. To prevent this non-physical behavior, Szilard and Pomraning suggest evaluating the opacities at a common cell-edge temperature. For example, in Eq. (21), we calculate $\sigma^{-}_{n,j+1/2}$ using the material properties in cell j and $\sigma^{+}_{n,j+1/2}$ using the material properties in cell $j+1$. However, from Ref. [20], the temperature used to evaluate both opacities is

$$T_{n,j+1/2} = \left(\frac{T^4_{n,j} + T^4_{n,j+1}}{2}\right)^{1/4}. \tag{23}$$

A similar technique can be used to calculate Eq. (20).

3.2. Interface cells

Next, we develop a method for interfacing DDMC with standard Monte Carlo by deriving a cell-centered equation for cell $j = 1$ on the left boundary of the DDMC region. A similar analysis can be performed for cell $j = J$. Writing Eq. (11) for $j = 1$ and using Eq. (18) for $F_{3/2}$ yields

$$\frac{1}{c}\frac{\mathrm{d}}{\mathrm{d}t}\phi_1 + (\sigma_{\mathrm{R},1} + f_{n,1}\sigma_{n,1})\phi_1 - \frac{1}{\Delta x_1}F_{1/2} = f_{n,1}\sigma_{n,1}acT_{n,1}^4 + \frac{1}{\Delta x_1}\sigma_{\mathrm{L},2}\phi_2\Delta x_2. \tag{24}$$

Here, we have made use of Eqs. (20) and (21). To complete this derivation, we must find an approximate expression for the flux at the boundary of the DDMC region.

Instead of using the usual Marshak boundary condition [15,20], we consider the asymptotic diffusion-limit boundary condition [14]:

$$2\int_0^1 W(\mu)I_b(\mu,t)\,\mathrm{d}\mu = \phi(X_\mathrm{L},t) - \frac{\lambda}{\sigma_n}\left.\frac{\partial\phi}{\partial x}\right|_{x=X_\mathrm{L}}. \tag{25}$$

In Eq. (25), $I_b(\mu,t)$ is the radiation intensity due to Monte Carlo particles incident on the DDMC region, while $\lambda \approx 0.7104$ is the *extrapolation distance*. In addition, $W(\mu)$ is a transcendental function well approximated by[1]

$$W(\mu) \approx \mu + \frac{3}{2}\mu^2. \tag{26}$$

Eq. (25) can be derived in an asymptotic analysis of Eq. (3) as σ_n becomes large and f_n becomes small. This is exactly the situation in which DDMC is employed. Also, the incident intensity is weighted by $W(\mu)$, a function that takes into account the angular distribution of the incoming Monte Carlo particles. An interface method based on Eq. (25) will be able to produce accurate results in the interior of the DDMC region even if the incident radiation is anisotropic [12,13]. In contrast, the Marshak boundary condition treats all angular distributions identically and can produce inaccurate solutions for strongly anisotropic Monte Carlo particles [12,13].

To express $F_{1/2}$ using Eq. (25), we approximate the derivative on the right side with a finite difference. We then have

$$2\int_0^1 W(\mu)I_b(\mu,t)\,\mathrm{d}\mu = \phi_{1/2} - \frac{2\lambda}{\sigma_{n,1}\Delta x_1}(\phi_1 - \phi_{1/2}), \tag{27}$$

where $\sigma_{n,1}$ is the explicitly evaluated cell-averaged opacity in cell $j = 1$, and $\phi_{1/2}$ is an appropriately defined cell-edge scalar intensity. Solving Eq. (27) for $\phi_{1/2}$ yields

$$\phi_{1/2} = \frac{2\lambda}{\sigma_{n,1}\Delta x_1 + 2\lambda}\phi_1 + \frac{2\sigma_{n,1}\Delta x_1}{\sigma_{n,1}\Delta x_1 + 2\lambda}\int_0^1 W(\mu)I_b(\mu,t)\,\mathrm{d}\mu. \tag{28}$$

Next, we use Eq. (16) to represent $F_{1/2}$,

$$F_{1/2} = -\frac{2}{3\sigma_{n,1}\Delta x_1}(\phi_1 - \phi_{1/2}), \tag{29}$$

where we have evaluated the face-averaged opacity with the cell-averaged value, i.e.,

$$\sigma_{n,1/2}^{+} = \sigma_{n,1}. \tag{30}$$

When we substitute Eq. (28) into Eq. (29), we find that an expression for the flux at the boundary of the DDMC region is

$$F_{1/2} = -\frac{2}{3\sigma_{n,1}\Delta x_1 + 6\lambda}\left(\phi_1 - 2\int_0^1 W(\mu)I_b(\mu,t)\,\mathrm{d}\mu\right). \tag{31}$$

Using Eq. (31) in Eq. (24) yields the DDMC equation for cell $j = 1$:

$$\frac{1}{c}\frac{\mathrm{d}}{\mathrm{d}t}\phi_1 + (\sigma_{\mathrm{L},1} + \sigma_{\mathrm{R},1} + f_{n,1}\sigma_{n,1})\phi_1 = f_{n,1}\sigma_{n,1}acT_{n,1}^4 + \frac{1}{\Delta x_1}\left(\sigma_{\mathrm{L},2}\phi_2\Delta x_2 + \int_0^1 P(\mu)\mu I_b(\mu,t)\,\mathrm{d}\mu\right). \tag{32}$$

Here, the left-leakage opacity is given by

[1] One reviewer pointed out that another approximation, which may be more accurate in some applications and could easily be implemented into our existing methodology, is $W(\mu) = 0.91\mu + 1.635\mu^2$.

$$\sigma_{\mathrm{L},1} = \frac{1}{\Delta x_1}\frac{2}{3\sigma_{n,1}\Delta x_1 + 6\lambda}, \tag{33}$$

instead of Eq. (20), and $P(\mu)$ is defined as

$$P(\mu) = \frac{4}{3\sigma_{n,1}\Delta x_1 + 6\lambda}\left(1 + \frac{3}{2}\mu\right). \tag{34}$$

Eq. (32) has a Monte Carlo interpretation similar to that of Eq. (19). The only difference on the left side is the expression for the left-leakage opacity. On the right side, there is now a source due to Monte Carlo particles incident on the boundary of the DDMC region. We note that the rate at which radiation energy is incident on the DDMC region boundary for a given direction μ is μI_b. Then, $P(\mu)$ has the interpretation of being the probability that an incoming Monte Carlo particle with direction μ is converted into a DDMC particle. This interface methodology is similar to the treatment developed by Brockway for combining Monte Carlo and deterministic diffusion calculations [21]. However, our technique has a direction-dependent conversion probability and is based on the asymptotic diffusion-limit boundary condition, whereas Brockway's employs an angularly independent conversion probability and is developed from the Marshak boundary condition.

We implement the conversion of Monte Carlo particles into DDMC particles in two separate ways. First, if the DDMC region is away from the problem boundary (for example, $X_{\mathrm{L}} \neq 0$), we sample based on Eq. (34) to determine if the incident Monte Carlo particle is converted. If the particle is converted, it begins transporting via DDMC in cell $j = 1$. Otherwise, the particle is returned isotropically to the optically thin region. DDMC particles that undergo left-leakage reactions in cell $j = 1$ are also placed isotropically on the boundary of the DDMC region. This angular distribution is only correct when the incident intensity is isotropic and may be very inaccurate for small exiting angles (i.e., when the cosine between the particle direction and surface normal is small). However, particles with these small angles have the least impact on the solution, and in general, this isotropic angular distribution can be shown to be a good approximation [22]. We are currently investigating the use of more accurate angular distributions [23].

Second, if the DDMC region is on the boundary of the system (for example, $X_{\mathrm{L}} = 0$), then the incoming Monte Carlo particles are actually source particles due to a prescribed incident intensity. In this case, we split the particles according to Eq. (34). That is, a fraction $P(\mu)$ of the particle is converted into a DDMC particle and begins transporting via DDMC in cell $j = 1$, while the remaining fraction $1 - P(\mu)$ is tallied as escaping energy. DDMC particles that experience left-leakage reactions in cell $j = 1$ are also counted as escaping energy.

There are two difficulties when evaluating the conversion probability, Eq. (34). First, the conversion probability, along with the left-leakage opacity given by Eq. (33), vanishes when the opacity becomes large. Thus, no radiation can pass through the DDMC region boundary if the first cell is too optically thick. We correct this situation by adjusting the conversion probability and leakage opacity to ensure that an accurate flux is preserved at the boundary. For brevity we do not repeat this analysis here; a full description is given in Ref. [24]. In addition, Eq. (34) must have a valid probabilistic interpretation, i.e.,

$$0 \leqslant P(\mu) \leqslant 1, \quad 0 < \mu \leqslant 1. \tag{35}$$

In our DDMC implementation, we require that spatial cells are large enough such that Eq. (35) is always satisfied.

3.3. Estimation of momentum deposition

Coupled radiation-hydrodynamics calculations require estimates of the radiation energy *and* the radiation momentum deposited in the material. The estimation of energy deposition in DDMC is the same as in standard Monte Carlo; when a particle is absorbed, its energy is allocated to the material. The momentum deposition is given by Eq. (7),

$$p(x,t) = \frac{\sigma}{c}\int_{-1}^{1} \mu I(x,\mu,t)\,\mathrm{d}\mu, \tag{36}$$

and is straightforward to estimate in a standard Monte Carlo simulation. However, the estimation of momentum deposition in DDMC is difficult since there is no angular information to evaluate Eq. (36).

Instead, we use Eq. (10) to write Eq. (36) as a function of the radiative flux at a surface. For example, at $x = x_{j+1/2}$, we can express the momentum deposition as

$$p_{j+1/2} = \frac{\sigma_{n,j+1/2}}{c} F_{j+1/2}, \tag{37}$$

where we have employed a time-explicit, face-averaged value for the opacity. Then, for each cell, we average the two cell-edge values of the momentum deposition in order to estimate the cell-averaged value,

$$p_j = \frac{1}{2c}(\sigma^+_{n,j-1/2} F_{j-1/2} + \sigma^-_{n,j+1/2} F_{j+1/2}). \tag{38}$$

Note that we have evaluated Eq. (37) using the same face-averaged opacities used to calculate the leakage opacities [Eqs. (20), (21), and (33)].

The radiative flux in Eq. (38) can easily be calculated during a DDMC simulation. For cells interior to the DDMC region, we can express Eq. (18) using Eqs. (20) and (21) as

$$F_{j+1/2} = \sigma_{\mathrm{R},j} \phi_j \Delta x_j - \sigma_{\mathrm{L},j+1} \phi_{j+1} \Delta x_{j+1}. \tag{39}$$

Eq. (39) is the rate at which radiation energy undergoes right-leakage reactions in cell j, minus the rate at which radiation energy experiences left-leakage reaction in cell $j+1$. Similarly, we can write Eq. (31) using Eqs. (33) and (34) as

$$F_{1/2} = \int_0^1 P(\mu) \mu I_b(\mu, t)\, \mathrm{d}\mu - \sigma_{\mathrm{L},1} \phi_1 \Delta x_1. \tag{40}$$

We view Eq. (40) as the rate that incident radiation energy enters the DDMC region, minus the rate that radiation energy undergoes left-leakage reactions in cell $j = 1$. Contributions to the time-step averages of Eqs. (39) and (40) are tallied each time a DDMC particle moves to a new cell. Then, at the end of the time step, these estimates of the cell-edge fluxes can be used to evaluate Eq. (38) and calculate the momentum deposition for each DDMC spatial cell.

4. Numerical results

We now demonstrate the accuracy and improved efficiency, with respect to standard Monte Carlo and RW, of our new DDMC method using a series of IMC simulations. In these problems, we measure energy in gigajoules (gJ), time in nanoseconds (ns), and temperature in kiloelectron-volts (keV). In addition, the material has a temperature-independent heat capacity of $C_v = 0.1$ gJ/cm^3/keV, and, unless otherwise stated, an opacity inversely proportional to the cube of the material temperature,

$$\sigma = \frac{\sigma_0}{T^3}. \tag{41}$$

In the following simulations we use several values of σ_0 to test our improved DDMC method under various conditions.

4.1. Infinite medium problems

In the first set of problems, we examine a 1-cm-thick slab with reflective boundary conditions. The matter and radiation are initially in equilibrium at 1 keV and should remain in equilibrium indefinitely. We use a cell size of 0.01 cm, a time-step size of 0.1 ns, and 10,000 particles per time step. For each value of σ_0, we ran the simulation for an elapsed time of 10 ns using either DDMC or standard Monte Carlo over the entire problem domain.

Every simulation, both standard Monte Carlo and DDMC, retained the correct equilibrium solution. The timing results for these calculations are given in Table 1. Here, we have defined speedup as the computer time required by standard Monte Carlo divided by that required by DDMC. From these results, we see that

Table 1
Infinite medium timing results

σ_0 (keV^3/cm)	Monte Carlo time (s)	DDMC time (s)	Speedup
100	670	197	3.4
500	2.70×10^3	47	57
1000	5.25×10^3	27	190
5000	2.56×10^4	12	2100
10,000	5.11×10^4	10	5100

DDMC always increases the efficiency of the IMC calculation, from a factor of about 3 to more than 5000. As expected, DDMC becomes more efficient relative to standard Monte Carlo as the opacity becomes larger. In fact, the DDMC timings decrease with increasing opacity due to more absorption and less leakage from each spatial cell.

4.2. Thermal waves

The next set of problems consists of thermal waves driven by a 1 keV intensity incident on the left boundary of the system. The material and radiation are initially in equilibrium at 1.0×10^{-6} keV. In these simulations, the cell size is 0.005 cm, the time-step size is 0.01 ns, and we use 100,000 particles per time step. With this spatial discretization, cell sizes range from 5.0×10^{19} mean-free paths for the largest value of σ_0 considered at the initial temperature, to 5 mean-free paths for the smallest value of σ_0 at the source temperature. Again, for each value of σ_0 we performed the IMC calculation using standard Monte Carlo or DDMC throughout the entire problem and ran each simulation for an elapsed time of 10 ns.

We first consider thermal waves in a case where the incident intensity is isotropic. The timing results from these simulations are presented in Table 2. From this table we see that DDMC improves the efficiency of the IMC calculation, and the efficiency improvement increases with increasing opacity. For these problems, the speedup ranged from about 40 to more than 400.

We also plot the material temperature and momentum deposition at 10 ns for $\sigma_0 = 1000$ keV^3/cm in Figs. 1 and 2, respectively. These plots are characteristic of the results for other values of σ_0. From Fig. 1, we see that the DDMC temperature agrees well with the standard Monte Carlo solution. Also, as seen in Fig. 2, the momentum-deposition results tend to match, especially near the wave front. However, both the DDMC and standard Monte Carlo momentum-deposition estimates suffer from severe statistical noise. This large amount of statistical error is characteristic of momentum-deposition calculations.

Next, we examine thermal waves driven by a normally incident intensity. This anisotropic incident intensity will induce a boundary layer and test the effectiveness of our improved interface method. The timing results for these simulations are given in Table 3. Again, DDMC is more efficient than standard Monte Carlo, and the efficiency gain is greater for larger opacities.

The material temperature and momentum deposition at 10 ns for $\sigma_0 = 1000$ keV^3/cm are plotted in Figs. 3 and 4, respectively. As with the isotropic intensity problems, these plots are characteristic of the results for other values of σ_0. From these figures we see that the DDMC solution matches the Monte Carlo results quite well. Again, both estimates of momentum deposition suffer from high statistical error. Although the maximum material temperature is greater than 1 keV, this calculation does not violate the maximum principle as the incident intensity is anisotropic [2,25,26]. We also note that in Fig. 3 there is a boundary layer in the Monte Carlo solution near the left boundary. Although this boundary layer is absent in the DDMC solution, there does not

Table 2
Isotropic incident intensity timing results

σ_0 (keV^3/cm)	Monte Carlo time (s)	DDMC time (s)	Speedup
1000	5.40×10^4	1.09×10^3	49.5
5000	2.05×10^5	8.06×10^2	254
10,000	3.59×10^5	7.82×10^2	459

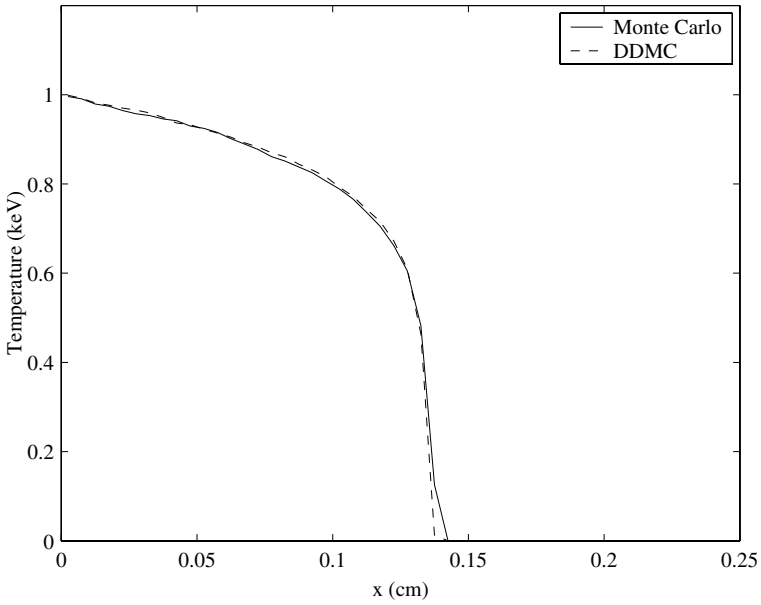

Fig. 1. Isotropic incident intensity material temperature, $\sigma_0 = 1000\ \mathrm{keV}^3/\mathrm{cm}$.

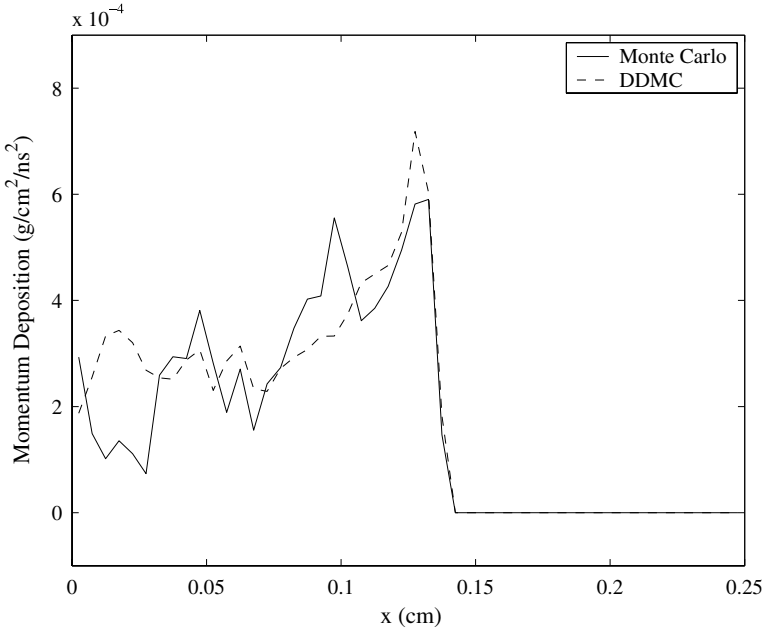

Fig. 2. Isotropic incident intensity momentum deposition, $\sigma_0 = 1000\ \mathrm{keV}^3/\mathrm{cm}$.

appear to be a statistically significant difference between the DDMC and Monte Carlo leakage rates for this problem.

In addition, we test the ability of our improved interface method to treat a grazing incident intensity. In this case, the incident radiation is aligned in the $\mu = 0.1$ direction. As with the normally incident intensity thermal waves considered above, these simulations provide another examination of the accuracy of the approximate $W(\mu)$ given by Eq. (26). The timing results for these grazing incident intensity problems are given in Table 4.

Table 3
Normally incident intensity timing results

σ_0 (keV^3/cm)	Monte Carlo time (s)	DDMC time (s)	Speedup
1000	5.12×10^4	1.15×10^3	44.5
5000	1.99×10^5	7.89×10^2	252
10,000	3.56×10^5	7.46×10^2	477

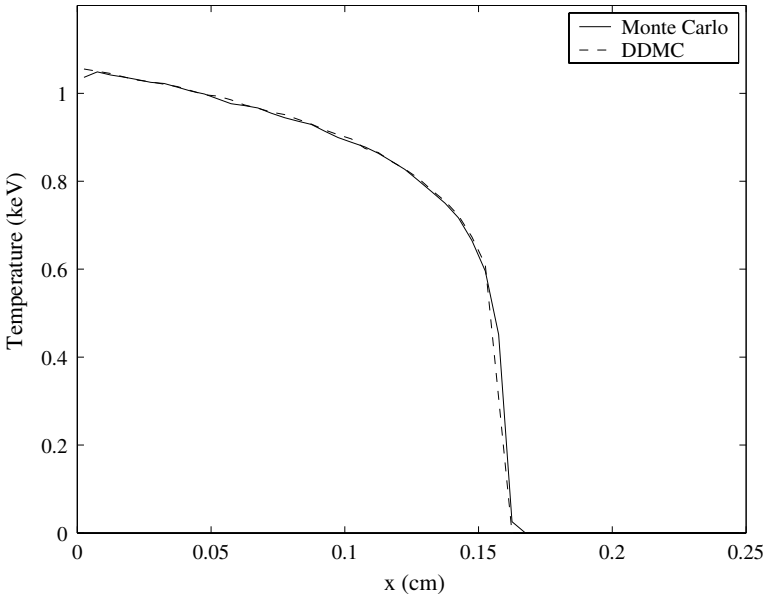

Fig. 3. Normally incident intensity material temperature, $\sigma_0 = 1000$ keV^3/cm.

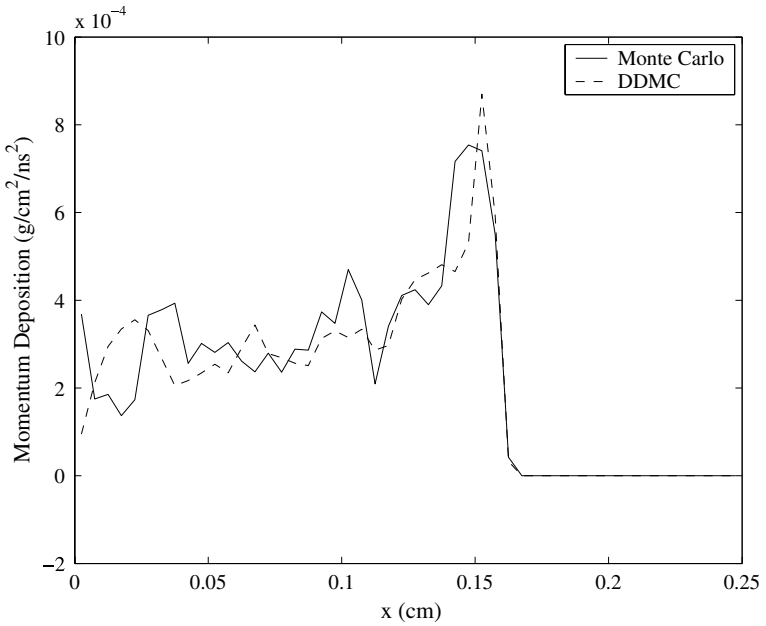

Fig. 4. Normally incident intensity momentum deposition, $\sigma_0 = 1000$ keV^3/cm.

Table 4
Grazing incident intensity timing results

σ_0 (keV^3/cm)	Monte Carlo time (s)	DDMC time (s)	Speedup
1000	6.02×10^4	9.65×10^2	62.4
5000	2.11×10^5	8.35×10^2	253
10,000	3.58×10^5	8.30×10^2	431

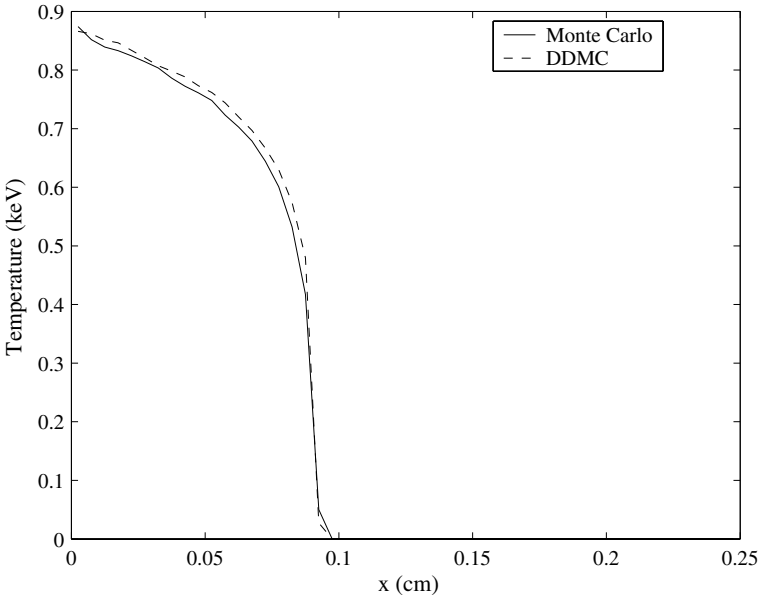

Fig. 5. Grazing incident intensity material temperature, $\sigma_0 = 1000$ keV^3/cm.

As with the other thermal-wave simulations, DDMC is more efficient than standard Monte Carlo, and efficiency improvement increases with increasing opacity.

We plot the material temperature and momentum deposition at 10 ns for $\sigma_0 = 1000$ keV^3/cm in Figs. 5 and 6, respectively. Again, these figures are characteristic of the results for other values of σ_0. In these plots, the DDMC results agree well with the standard Monte Carlo solutions, although not as well as in the isotropic and normally incident intensity problems. Specifically, the DDMC material temperature is slightly higher than the Monte Carlo results in Fig. 5, and DDMC overestimates the momentum deposition in Fig. 6—more so than in Figs. 2 and 4. This decrease in accuracy is most likely caused by the inaccuracy of Eq. (26) for small values of μ. As with the normally incident intensity simulation, the boundary layer near the left boundary in Fig. 5 does not cause a discrepancy between the DDMC and Monte Carlo leakage rates.

In Fig. 7, we replot the DDMC material temperatures from Figs. 1, 3, and 5. From this plot we note that the normally incident intensity material temperature is higher, and the wave has progressed farther; and the grazing incident intensity material temperature is lower, and the wave has not progressed as far, as compared to the isotropic incident intensity results. If we had employed the Marshak boundary condition as opposed to the asymptotic diffusion-limit boundary condition to develop our interface method, all DDMC solutions in Fig. 7 would be identical to the isotropic incident intensity solution and thus incorrect for the other two angular distributions considered. This inaccuracy is caused by the inability of the Marshak boundary condition to differentiate between anisotropic angular distributions; the Marshak boundary condition treats the incident radiation energy as if it were distributed isotropically. Readers are directed to Refs. [12,13] for a more systematic comparison of interface methods based on the Marshak and asymptotic diffusion-limit boundary conditions.

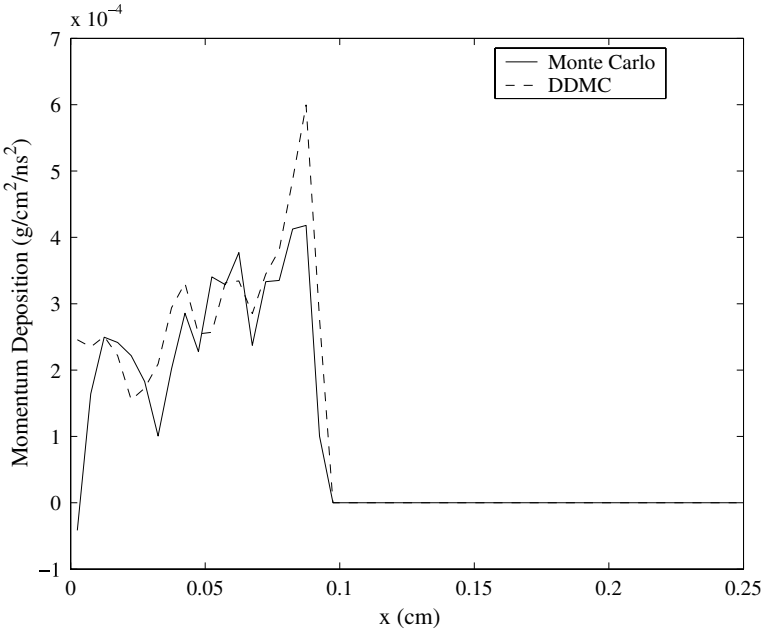

Fig. 6. Grazing incident intensity momentum deposition, $\sigma_0 = 1000\ \text{keV}^3/\text{cm}$.

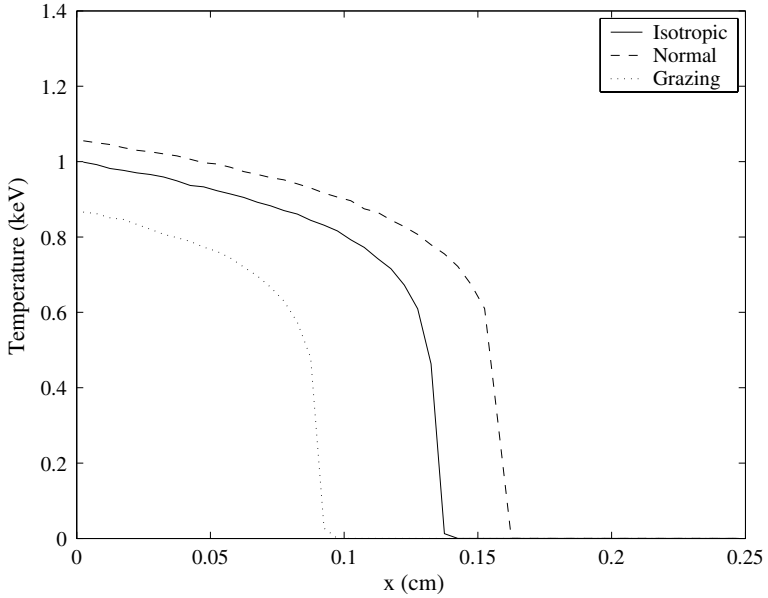

Fig. 7. Comparison of DDMC material temperatures for different incident angular distributions.

4.3. Hybrid problems

We now consider two problems with both optically thick and optically thin regions. We model the optically thick region using an opacity given by Eq. (41) with $\sigma_0 = 1000\ \text{keV}^3/\text{cm}$. The optically thin region has a temperature-independent opacity of $1\ \text{cm}^{-1}$. The material and radiation are initially in equilibrium at 1.0×10^{-6} keV, and the left boundary has an incident intensity at 1 keV. In these simulations, the cell thickness

is 0.005 cm in the optically thick region and 0.02 cm in the optically thin region, the time-step size is 0.01 ns, and we use 100,000 particles per time step.

To simulate these problems we employed standard Monte Carlo in the optically thin region and either standard Monte Carlo or DDMC in the optically thick region. The pure Monte Carlo calculation serves as our benchmark solution, while the hybrid Monte Carlo-DDMC simulation will test the accuracy and efficiency of DDMC.

In the first problem, the incident intensity is isotropic, the leftmost region ($0\text{ cm} < x < 0.1\text{ cm}$) is optically thick, and the rightmost region ($0.1\text{ cm} < x < 0.5\text{ cm}$) is optically thin. The right boundary is reflective such that the problem will eventually reach equilibrium at 1 keV. We ran each simulation to an elapsed time of 150 ns.

The material temperature at 10, 20, and 150 ns is plotted in Fig. 8. From this figure we see that the DDMC results agree well with the standard Monte Carlo solution, and both methods produce the correct equilibrium solution. In Fig. 9, we plot the momentum deposition at 10 ns. From this plot it appears the DDMC simulation overestimates the peak momentum deposition with respect to standard Monte Carlo by a factor of two. One possible explanation for this error is that DDMC estimates momentum deposition at cell edges, while standard Monte Carlo estimates momentum deposition as a cell average. However, this explanation is not completely sufficient, because DDMC produced momentum-deposition estimates that agreed well with the corresponding Monte Carlo solutions in the thermal waves discussed above. Certainly, the accuracy of our technique for estimating momentum deposition should be studied over a wider range of problems. For this problem, the standard Monte Carlo simulation required 120 h of computer time, while DDMC used 5.6 h—a speedup of greater than 20.

In the second problem, the prescribed intensity is normally incident, the leftmost region ($0\text{ cm} < x < 1\text{ cm}$) is optically thin, and the rightmost region ($1\text{ cm} < x < 1.5\text{ cm}$) is optically thick. We ran each simulation to an elapsed time of 50 ns. Since the optically thin region is a mean-free path thick, the intensity reaching the optically thick region is fairly anisotropic. Thus, using our improved interface method is important for this problem.

The resulting material temperature at 0.5, 1.5, and 50 ns is plotted in Fig. 10. Again, the DDMC results agree well with the standard Monte Carlo solution. As in the normally incident thermal wave case discussed above, this calculation does not violate the maximum principle, even though the material temperature is

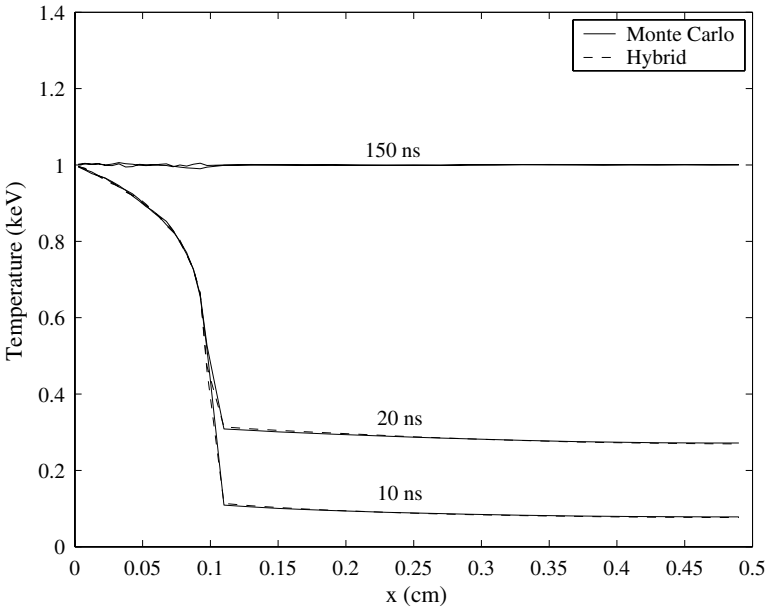

Fig. 8. First hybrid problem material temperature.

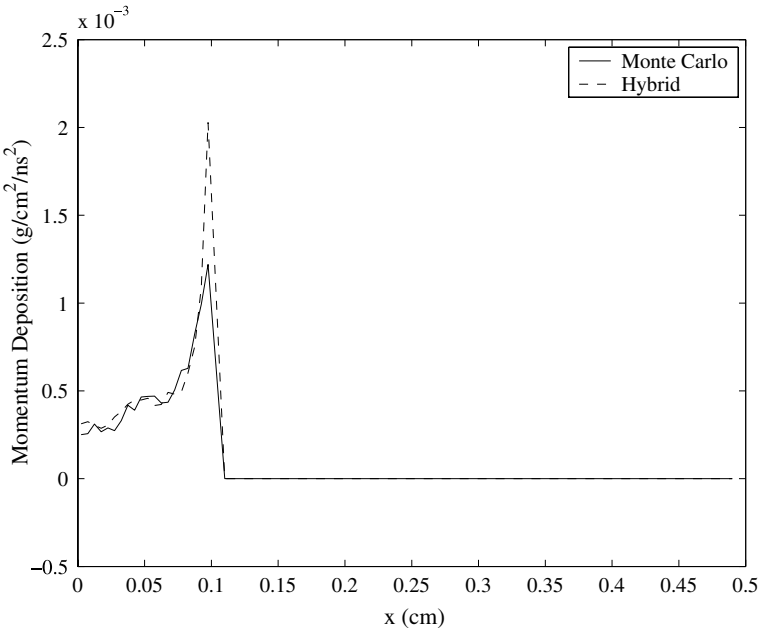

Fig. 9. First hybrid problem momentum deposition.

greater than 1 keV, due to the anisotropic incident intensity. In addition, we plot the momentum deposition at 0.5 ns in Fig. 11. Most momentum deposition occurred in only a few cells near the interface between the optically thin and optically thick regions. However, the DDMC estimate was within 1.6% of the standard Monte Carlo solution at the peak value. In this problem, standard Monte Carlo took 28.6 h of computer time, while DDMC required 2.2 h—for a speedup of about 13.

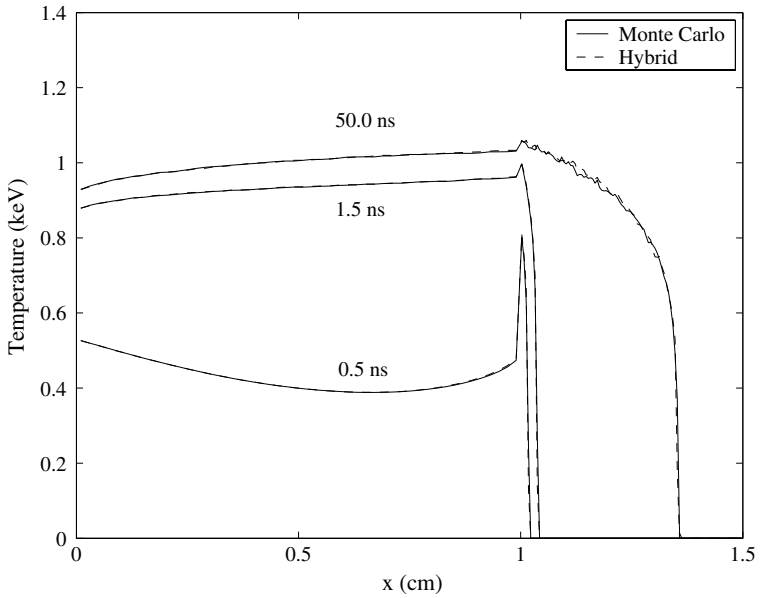

Fig. 10. Second hybrid problem material temperature.

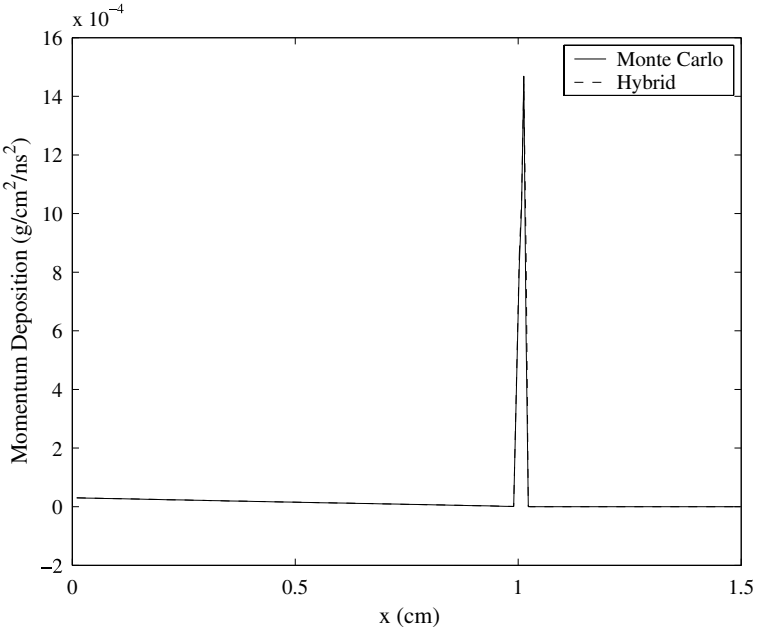

Fig. 11. Second hybrid problem momentum deposition.

4.4. Comparison of DDMC and RW

We now compare our DDMC method to RW. In RW, the sphere radius R is required to be greater than five effective-scattering mean-free paths [6], i.e.,

$$R > \frac{5}{(1-f_n)\sigma_n}. \tag{42}$$

Otherwise, the particle is transported via standard Monte Carlo. This requirement would cause RW to be invoked infrequently, if at all, in the radiative-transfer problems presented previously. Thus, we compare DDMC to RW using a new radiative-transfer problem. This problem has an optically thick region adjacent to an optically thin region and reflective boundary conditions. The optically thick region ($0\text{ cm} < x < 1\text{ cm}$) has an opacity given by Eq. (41) with $\sigma_0 = 50{,}000\text{ keV}^3/\text{cm}$. The optically thin region ($1\text{ cm} < x < 2\text{ cm}$) has a temperature-independent opacity of 1 cm^{-1}. The material and radiation are initially in equilibrium at 1 keV and should remain in equilibrium indefinitely. We use 10,000 particles per time step, a time-step size of 0.1 ns, a cell size of 0.1 cm in the optically thin region, and various cell sizes in the optically thick region. We performed each calculation using standard Monte Carlo in the optically thin region, and standard Monte Carlo, RW, or DDMC in the optically thick region. In addition, we ran each simulation for an elapsed time of 10 ns.

Every method (pure Monte Carlo, hybrid Monte Carlo/RW, and hybrid Monte Carlo/DDMC) preserved the correct equilibrium solution regardless of cell size. The timing results for these calculations are presented in Table 5. Here, we have defined speedup as the computer time required by standard Monte Carlo divided by the computer time required for the given hybrid method. From this table, we see that both RW and DDMC are more efficient than standard Monte Carlo, and DDMC is more efficient than RW for all cell sizes. RW performs the best for optically thick spatial cells, since the sphere radii are large and Eq. (42) is more easily satisfied. However, for the largest cell size considered, $\Delta x = 0.1$ cm, the DDMC calculation was still about 18 times faster than the RW simulation. As the spatial grid is refined in the optically thick region, the efficiency gain of each hybrid method decreases. However, the decrease in speedup is much greater for RW than DDMC. For small cell sizes, DDMC particles still take discrete steps across spatial cells (albeit small steps), and RW is invoked infrequently. Thus, we expect DDMC to perform better than RW as cell size decreases.

Table 5
Comparison of DDMC and RW

Δx (cm)	Monte Carlo time (s)	RW time (s)	RW speedup	DDMC time (s)	DDMC speedup
0.1	1.49×10^5	299	498	16	9300
0.05	1.48×10^5	589	251	16	9300
0.01	1.49×10^5	2.88×10^3	51.7	18	8300
0.005	1.50×10^5	5.79×10^3	25.9	19	7900
0.001	1.60×10^5	3.14×10^4	5.1	53	3000

For the smallest cell size considered, $\Delta x = 0.001$ cm, the DDMC calculation was almost 600 times faster than the RW simulation.

5. Conclusions

We have extended previously developed DDMC methods in three ways that improve the accuracy and utility of DDMC for grey IMC simulations. First, our DDMC method employs a temporally continuous diffusion equation. This lack of temporal discretization results in a theoretically more accurate DDMC calculation and no ambiguity regarding what time to assign to DDMC particles that are converted into Monte Carlo particles. Also, we use a technique for interfacing standard Monte Carlo and DDMC based on the asymptotic diffusion-limit boundary condition. This technique can produce accurate results regardless of the angular distribution of incident Monte Carlo particles. Finally, we develop a method for estimating momentum deposition in DDMC simulations. This momentum-deposition estimate is required to correctly calculate fluid motion in coupled radiation-hydrodynamics problems.

With a set of numerical calculations, we demonstrated the accuracy and improved efficiency, with respect to both standard Monte Carlo and RW, of our new DDMC method. Specifically, we observed speedups of 3–9000 over standard Monte Carlo and speedups of 18–600 over RW.

We note that although our temporally continuous treatment is theoretically more accurate than the use of a discretized diffusion equation in other DDMC techniques, we have not demonstrated this advantage numerically. The backward-Euler differencing employed in temporally discretized DDMC methods is first-order accurate in time, and thus is probably sufficient in most applications, while our temporally continuous DDMC technique is slightly more expensive due to the sampling of a time to collision (and evaluation of a logarithm) for every DDMC step. Nevertheless, our methodology is certainly superior at the interface between optically thick and optically thin regions since there is no need to assign a time to a DDMC particle that is converted into a Monte Carlo particle. As stated previously, temporally discretized DDMC techniques sample a time uniformly within a time step, and thus it is possible for the simulation to violate causality. Although it is uncertain what overall impact this non-physical behavior would have on a practical calculation, this effect is certainly undesirable. To investigate the possible advantages of our temporally continuous methodology in more detail, we plan on examining the treatment of transport-diffusion interfaces with respect to time in a way similar to the previous investigation done with respect to angle [13].

We have also neglected to develop a method for automatically determining what regions of the problem to simulate with DDMC, a requirement for employing DDMC in practical calculations. In the numerical results presented in this paper, the region in which we used DDMC was always selected *a priori*. Although there has been some effort to heuristically calculate the minimum allowable sphere size in RW [5,6], we are unaware of similar work for DDMC. When developing such a method, one must weigh accuracy versus efficiency gain when substituting DDMC for standard Monte Carlo. Thus, it is not only desirable to employ DDMC in a spatial cell if the cell itself is optically thick but also in an optically thick region consisting of several spatial cells even if the individual cells are of moderate optical depth. However, one should certainly not employ DDMC in optically thin spatial cells, even if the corresponding region is optically thick, since it is possible for DDMC to be less efficient than standard Monte Carlo in this case.

In addition to the areas of future work discussed above, there are several other issues that must be resolved in order for DDMC to be used in practical calculations. First, the estimates of momentum deposition exhibited a large amount of statistical error in both the DDMC and standard Monte Carlo simulations.

A technique for reducing this statistical error must be developed in order to accurately perform coupled radiation-hydrodynamics calculations. Also, the planar-geometry, grey DDMC method presented in this paper must be extend to multidimensional, frequency-dependent problems. This work would include developing a hybrid technique for treating optically thin and optically thick frequency groups and employing a diffusion equation discretized on the unstructured and/or non-orthogonal spatial grids commonly used in hydrodynamics calculations.

Acknowledgements

We would like to thank David Carrington (Los Alamos National Laboratory) for suggesting the use of face-averaged opacities when estimating momentum deposition. This work was performed under US government contract DE-AC52-06NA25396 for Los Alamos National Laboratory, which is operated by Los Alamos National Security, LLC. (LANS) for the US Department of Energy.

References

[1] J.A. Fleck Jr., J.D. Cummings, An Implicit Monte Carlo scheme for calculating time and frequency dependent nonlinear radiation transport, J. Comput. Phys. 8 (1971) 313.
[2] E.W. Larsen, B. Mercier, Analysis of a Monte Carlo method for nonlinear radiative transfer, J. Comput. Phys. 71 (1987) 50.
[3] W.R. Martin, F.B. Brown, Error modes in Implicit Monte Carlo, Trans. Amer. Nucl. Soc. 85 (2002) 508.
[4] S.W. Mosher, J.D. Densmore, Stability and monotonicity conditions for linear, grey, 0-D Implicit Monte Carlo calculations, Trans. Amer. Nucl. Soc. 93 (2005) 520.
[5] J.A. Fleck Jr., E.H. Canfield, A random walk procedure for improving the computational efficiency of the Implicit Monte Carlo method for nonlinear radiation transport, J. Comput. Phys. 54 (1984) 508.
[6] J. Giorla, R. Sentis, A random walk method for solving radiative transfer equations, J. Comput. Phys. 70 (1987) 145.
[7] T.J. Urbatsch, J.E. Morel, J. Gulick, Monte Carlo solution of spatially-discrete transport equations, Part II: Diffusion and transport-diffusion, in: Proceedings of the International Conference on Mathematics and Computation, Reactor Physics, and Environmental Analysis in Nuclear Applications, Madrid, Spain, 27–30 September 1999, vol. 1, p. 262.
[8] T.M Evans, T.J. Urbatsch, H. Lichtenstein, 1-D equilibrium Discrete Diffusion Monte Carlo, in: Proceedings of MC2000—International Conference, Lisbon, Portugal, July, 2000.
[9] N.A. Gentile, Implicit Monte Carlo Diffusion—an acceleration method for Monte Carlo time-dependent radiative transfer simulations, J. Comput. Phys. 172 (2001) 543.
[10] J.D. Densmore, T.J. Urbatsch, T.M. Evans, M.W. Buksas, Discrete Diffusion Monte Carlo for grey Implicit Monte Carlo simulations, in: Proceedings of the International Topical Meeting on Mathematics and Computation, Supercomputing, Reactor Physics and Nuclear and Biological Applications, Avignon, France, 12–15 September 2005.
[11] E.W. Larsen, G.C. Pomraning, V.C. Badham, Asymptotic analysis of radiative transfer problems, J. Quant. Spectrosc. Radiat. Transfer 29 (1983) 285.
[12] J.D. Densmore, An improved method for treating Monte Carlo-diffusion interfaces, Trans. Amer. Nucl. Soc. 91 (2004) 139.
[13] J.D. Densmore, Interface methods for hybrid Monte Carlo-diffusion radiation transport simulations, Ann. Nucl. Energy 33 (2006) 343.
[14] G.J. Habetler, B.J. Matkowsky, Uniform asymptotic expansions in transport theory with small mean free paths, and the diffusion approximation, J. Math. Phys. 16 (1975) 846.
[15] G.I. Bell, S. Glasstone, Nuclear Reactor Theory, Krieger Publishing, Malabar, FL, 1985.
[16] D. Mihalas, B. Weibel-Mihalas, Foundations of Radiation Hydrodynamics, Dover Publications, Mineola, NY, 1999.
[17] J.I. Castor, Radiation Hydrodynamics, Cambridge University Press, Cambridge, UK, 2004.
[18] G.C. Pomraning, The Equations of Radiation Hydrodynamics, Pergamon Press, Oxford, UK, 1973.
[19] E.E. Lewis, W.F. Miller Jr., Computational Methods of Neutron Transport, American Nuclear Society, La Grange Park, IL, 1993.
[20] R.H. Szilard, G.C. Pomraning, Numerical transport and diffusion methods in radiative transfer, Nucl. Sci. Eng. 112 (1992) 256.
[21] G.C. Pomraning, G.M. Foglesong, Transport-diffusion interfaces in radiative transfer, J. Comput. Phys. 32 (1979) 420.
[22] C.J. Gesh, M.L. Adams, Finite element solutions of second-order forms of the transport equation at the interface between diffusive and non-diffusive regions, in: Proceedings of the International Meeting on Mathematical Methods for Nuclear Applications, Salt Lake City, UT, 9–13 September 2001.
[23] G. Davidson, J.D. Densmore, A.K. Prinja, J.E. Morel, Asymptotically correct angular distributions for Monte Carlo-diffusion interfaces, Trans. Amer. Nucl. Soc. 94 (2006) 517.
[24] J.D. Densmore, G. Davidson, D.B. Carrington, Emissivity of discretized diffusion problems, Ann. Nucl. Energy 33 (2006) 583.
[25] E.S. Andreev, M.Yu. Kozmanov, E.B. Rachilov, The maximum principle for a system of equations of energy and non-stationary radiation transfer, USSR Comput. Math. Math. Phys. 23 (1983) 104.
[26] B. Mercier, Application of accretive operators theory to the radiative transfer equations, SIAM J. Math. Anal. 18 (1987) 393.